Nonlinear spatiotemporal analysis and modeling of signal transduction pathways involving G protein coupled receptors

Chontita Rattanakul, Titiwat Sungkaworn , Yongwimon Lenbury, Meechoke Chudoung,
Varanuj Chatsudthipong, Wannapong Triampo, and Boriboon Novaprateep

Abstract— Cell behavior and communication are regulated by a complex network of intracellular and extracellular signal transduction pathways. In this paper, a model of signaling process involving G proteins is analyzed. The model incorporates reaction-diffusion mechanisms involving reactants that interact with each other on the cellular membrane surface and its proximity. The ligand-receptor complexes and the inhibiting agents in the process may diffuse over the cell membrane, and the signal transduction is mediated by the membrane bound G protein leading to biochemical intra-cellular reaction and the production of the second messenger or other desired functional responses. Weakly nonlinear stability analysis is carried out in order to investigate the dynamic and steady-state properties of the model. Turing-type patterns are shown to robustly form under conditions on the system parameters which characterize the formation of stationary symmetry breaking structures; stripes and hexagonal arrays of spots or nets. Some recent experimental studies are then mentioned in support of our theoretical predictions.

Keywords— Nonlinear analysis, signal transduction, Turing patterns, ligand-receptor complexes, reaction-diffusion equations.

C. Rattanakul is with the Department of Mathematics, Faculty of Science, Mahidol University, Bangkok 10400, Thailand and the Centre of Excellence in Mathematics, CHE, Bangkok 10400, Thailand (e-mail: sccrt@ mahidol.ac.th).

T. Sungkaworn is with the Department of Physiology, Faculty of Science, Mahidol University, Bangkok 10400, Thailand (e-mail: g5036089 @mahidol.ac.th).

Y. Lenbury is with the Department of Mathematics, Faculty of Science, Mahidol University, Bangkok 10400, Thailand and the Centre of Excellence in Mathematics, CHE, Bangkok 10400, Thailand (corresponding author; phone: 662-201-5448; fax: 662-201-5448; e-mail: scylb@ mahidol.ac.th).

M. Chudoung is with the Department of Mathematics, Faculty of Science, Mahidol University, Bangkok 10400, Thailand and the Centre of Excellence in Mathematics, CHE, Bangkok 10400, Thailand (e-mail: scmcd@ mahidol.ac.th).

V. Chatsudthipong is with the Department of Physiology, Faculty of Science, Mahidol University, Bangkok 10400, Thailand (e-mail: scvcs @mahidol.ac.th).

W. Triampo is with the Department of Physics, Faculty of Science, Mahidol University, Bangkok 10400, Thailand (e-mail: scwtr@ mahidol.ac.th).

B. Novaprateep is with the Department of Mathematics, Faculty of Science, Mahidol University, Bangkok 10400, Thailand and the Centre of Excellence in Mathematics, CHE, Bangkok 10400, Thailand (e-mail: scbnv@ mahidol.ac.th).

I. INTRODUCTION

Signal transduction at the cellular level refers to the movement of signals or flow of information from outside the cell to the inside. The movement of signals can be simple, such as that which involves the receptor molecules of the acetylcholine class. These receptors constitute channels which, upon ligand interaction, allow signals to pass, in the form of small ion movement, either into or out of the cell. The passage of ions leads to changes in the electrical potential of the cells that result in signals being propagated along the cell. More complex signal transduction involves the coupling of ligand-receptor interaction to various intracellular events. Thus, external stimuli are relayed to a series of internal reactants, which in turn trigger key cellular functions. A healthy functioning cell signaling mechanism is therefore essential for the well-being of the life form. Abnormalities of signal transduction pathways have been linked to the development of many serious disorders, such as Alzheimer's disease and cancer. Since hormones and their receptors are so closely related to carcinogenesis and several other diseases, better understanding of signal transduction mechanisms has been a subject of intense research [1-6].

In an earlier work, Rattanakul *et al.* [5] studied a model of the signal transduction pathway which involves G protein coupled receptors (GPCR), based on earlier investigations and modeling efforts of Spiegel [7], Levchenko and Iglesias [8], Rapple *et al.* [9], and Iglesias [1]. The reference model considered in the work of Rattanakul *et al.* [5] consists of a system of two differential equations which govern the interaction between an inhibitor protein (*I*) and the ligand-receptor complexes (*R*). Signal transduction across the cell membrane is mediated by membrane receptor bound proteins which connect the genetically controlled biochemical reactions in the cytosol to the production of the second messenger, eliciting desired intracellular responses. In their model [5], only the signaling hormone and, correspondingly, the ligand coupled receptors are allowed to diffuse over the extra-cellular membrane surface in two dimensions, while some transport of molecules across cell membrane (internalization) may take place to certain extent.

However, according to several studies [10-14] lateral diffusion coefficient of the inhibiting units of G protein in the

cytosol has been observed to be significantly higher than that of the membrane receptor complexes. Schlessinger *et al.* [14] reported that the protease inhibitors diffuse within the muscle fibers at the rate of $1 \, \mu m^2 / s$, while the lateral diffusion coefficients of ligand-receptor complexes were reported [15] to be in the range of $1.5 \times 10^{-2} - 8 \times 10^{-2} \, \mu m^2 / s$.

In the next section, we describe the essential stages of the cell signaling process: reception, transduction, and response, in which different reactants interact. From our detailed consideration of the process, we may derive the governing equations which will be analyzed in later sections. We utilize an optimization technique involving a genetic algorithm to estimate the values of the parameters in our model that yields simulation results which best fit the experimental data on the time series of the cAMP levels we have collected. The system is then modified to model the signal transduction pathway in which both reactants that take the major roles in the interactions, namely the inhibitor component and the ligand-receptor (LR) complexes, are allowed to diffuse over the two dimensional cell membrane surface and the plasmalemma. The fact that the diffusion rate of the inhibitor is significantly greater than that of the stimulator in our system permits the weakly nonlinear stability analysis of the model to be carried out to classify the dynamics and steady-state properties of model solutions. We show that Turing-type patterns will be formed robustly under different conditions imposed on the system parameters. In the last section, we discuss how certain connections can be made between reported experimental measurements and our predictions of different LR distribution patterns on the cell membrane. The theoretical predictions are then discussed in the contexts of recent experimental observations which have reported evidence that membrane spatial organization is an important contributor to the proper function of cell transduction of and response to external stimuli.

II. TRANSDUCTION PROCESS AND THE GOVERNING EQUATIONS

The proper functioning of a life form depends on the ability of its cellular constituents to communicate with each other. This requires that cells have a mechanism to detect and respond specifically to external signals [12]. One of the more complex strategies for doing this involves a three-stage G protein coupled enzyme cascade [16], a schematic description of which is shown in Figure 1.

In the first stage, the reception stage, a specialized membrane receptor protein is activated by its interaction with a particular ligand or absorbing a photon of light of a particular wavelength.

In the second stage, the transduction stage, the activated receptor, the density of which will be denoted R, turns on a heterotrimeric G protein, by causing the G protein to exchange GDP (guanosine diphosphate) for the nucleotide guanosine triphosphate (GTP) which activates the G protein. The α-subunit and the β-γ complex of the G protein then dissociate.

The GTP-bound α-subunit then diffuses along the membrane and binds to an effector (the adenylate cyclase or AC), activating it. This is followed by an appearance of GTPase activity resulting in the conversion of active α-GTP to inactive α-GDP and thereby inhibiting the activation of AC by G proteins.
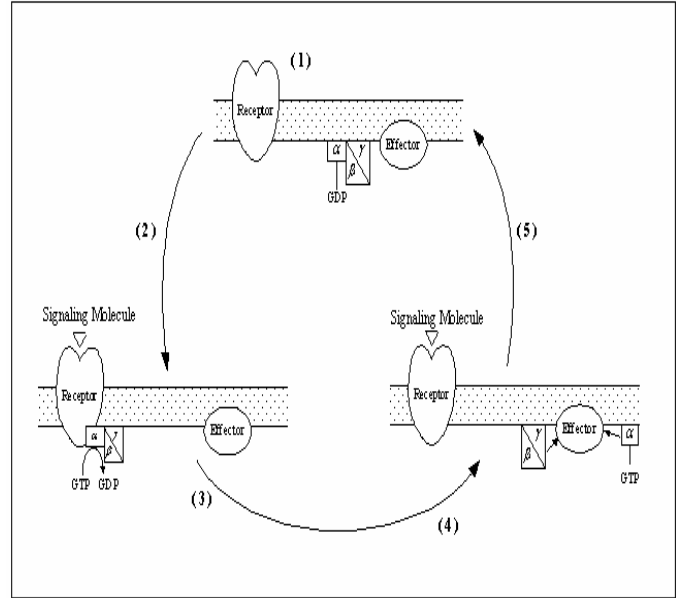

Fig. 1 Schematic diagram of the signal transduction process mediated by the G protein.

The GTP activating ligand (*A*) and the intrinsic GTPase enzymatic activity are thus able to function as a switch to sequentially turn on and turn off the signal transduction action of G protein α-subunits. In this mechanism we may therefore consider the GTP and GDP ligands to play the roles of activating agent (*A*) and inhibiting agent (*I*), respectively. Letting *G* be the amount of α-subunits of G proteins in the resting state, and *G** be that in the active state, *G* transforms to *G** according to the following reaction.

$$G \underset{I}{\overset{A}{\rightleftharpoons}} G* \tag{1}$$
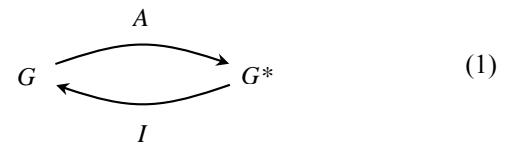
where the activating and inhibiting agents, whose densities are denoted *A* and *I*, respectively, are stimulated by the binding of ligands to receptors according to the following equations

$$\frac{dA}{dt} = -k_{-a}A + k_a R, \tag{2}$$

$$\frac{dI}{dt} = -k_{-i}I + k_i R, \tag{3}$$

where $R(t)$ is the membrane surface density of the ligand bound receptors (LR). Using mass action dynamics, an

equation for the transformation of G to $G*$ in (1) is

$$\frac{dG^*}{dt} = -k_{-r}IG^* + k_r AG. \tag{4}$$

Assuming that the total number $G_T = G + G^*$ of the regulators remains constant, (4) becomes

$$\frac{dG^*}{dt} = -[k_{-r}I + k_r A]G^* + k_r AG_T. \tag{5}$$

The active α-subunits of G proteins then associate with an effector protein, such as the membrane-bound adenylate cyclase (AC) enzyme (of amount E), to form a G_α-E complex of amount E^* that follows the equation

$$\frac{dE^*}{dt} = -k_{-e}E^* + k_e G^*, \tag{6}$$

and is stimulated by $G*$ to produce an intracellular response, such as the synthesis of cyclic AMP (adrenosine mono-phosphate), or a cyclic nucleotide or Ca2+ increase.

Letting C be the concentration of the second messenger, such as cAMP, which represents the output signal of the transduction process, then its strength is further amplified by each activated enzyme $E*$ [12]. Thus, we have

$$\frac{dC}{dt} = -k_{-c}C + k_c G^* E^* + k_c', \tag{7}$$

where the first term on the right corresponds to the removal rate while the last two terms are those of its synthesis, k_c' being the apparent zero order synthesis rate.

The cAMP in turns acts as a second messenger and amplifies the initial signal [17]. Thus, if no diffusion is in action and the LR complexes are distributed uniformly over the cell membrane, then the rate equation for the ligand-receptor complex density $R(t)$ on the cellular membrane surface at time t should read as follows

$$\frac{dR}{dt} = -\tilde{a}_3 R - \frac{\tilde{b}_1 R}{\tilde{b}_2 + R} + k_R C, \tag{8}$$

where the first term on the right is the removal rate, the second accounts for its transport through the cell membrane which saturates as the LR complex density R increases, and the third accounts for the signal amplification arising from the synthesis of cAMP.

Following previous works [1, 8], we now assume that the activated regulators G^*, E^*, and A equilibrate relatively quickly to the values

$$A = \frac{k_a}{k_{-a}} R, \tag{9}$$

$$G^* = \frac{G_T A}{A + k_R I}, \tag{10}$$

$$E^* = \frac{k_e G^*}{k_{-e}}, \tag{11}$$

where $k_R = \frac{k_{-r}}{k_r}$.

Substituting (9) into (10), one obtains

$$G^* = \frac{\tilde{k}R}{\tilde{b}_3 R + I}, \tag{12}$$

where $\tilde{k} = \frac{G_T k_a}{k_R k_{-a}}$, and $\tilde{b}_3 = \frac{k_a}{k_{-a} K_R}$.

Further, it has also been discovered [7] that the cAMP also equilibrates very rapidly, in comparison to the ligand bound receptor complexes or the inhibitors. Thus, on putting $\frac{dC}{dt} = 0$, and using (12), one arrives at

$$C = \frac{\tilde{b}_4 R^2}{\left(\tilde{b}_3 R + I\right)^2} + K_C \tag{13}$$

at equilibrium, where

$$\tilde{b}_4 = \frac{k_c k_e \tilde{k}}{k_{-c} k_{-e}},$$

and

$$K_C = \frac{k_c'}{k_{-c}}.$$

Substituting (13) into (8), one arrives at the following system:

$$\frac{\partial I}{\partial t} = -k_{-i}I + k_i R, \tag{14}$$

$$\frac{\partial R}{\partial t} = -\tilde{a}_3 R - \frac{\tilde{b}_1 R}{\tilde{b}_2 + R} + \frac{k_R \tilde{b}_4 R^2}{\left(\tilde{b}_3 R + I\right)^2} + k_R K_C. \tag{15}$$

Next, we introduce scaling factors by letting

$[G_i]_T$ = total concentration per cell of $G_{\alpha i}$ (μmol·m^{-2}),

$[G_s]_T$ = total concentration per cell of $G_{\alpha s}$ (μmol·m^{-2}),

$t*$ = time scaling factor in seconds.

If we now let $\hat{I}, \hat{R}$, and τ be dimensionless space and time variables as follows

$$\hat{I} = \frac{I}{[G_i]_T},$$

$$\hat{R} = \frac{R}{[G_s]_T},$$

and $\tau = \frac{t}{t^*}$, then we arrive at the following system:

$$\frac{\partial \hat{I}}{\partial \tau} = -a_1 \hat{I} + a_2 \hat{R}, \tag{16}$$

$$\frac{\partial \hat{R}}{\partial \tau} = -a_3 \hat{R} - \frac{b_1 \hat{R}}{b_2 + \hat{R}} + \frac{a_4 \hat{R}^2}{\left(a_5 \hat{R} + \hat{I}\right)^2} + a_6, \tag{17}$$

and

$$C = \frac{b_3 \hat{R}^2}{(a_5 \hat{R} + \hat{I})^2} + K_C, \tag{18}$$

where $a_1 = t^*\left[G_i\right]_T k_{-i}$, $a_2 = t^*\left[G_s\right]_T k_i$, $\text{a}_3 = t^*\left[G_s\right]_T \tilde{a}_3$,

$$a_4 = \frac{t^*\left[G_s\right]_T^2}{\left[G_i\right]_T^2}\tilde{b}_4 k_R, a_5 = \frac{\left[G_s\right]_T}{\left[G_i\right]_T}\tilde{b}_3, a_6 = t^* k_R K_C,$$

$$b_1 = t^*\tilde{b}_1, \quad b_2 = \frac{\tilde{b}_2}{\left[G_s\right]_T}, \text{ and } b_3 = \frac{t_b\left[G_s\right]_T^2}{\left[G_i\right]_T^2}\tilde{b}_4.$$

III. PARAMETERS ESTIMATION BY GENETICS ALGORITHM

To determine whether the above system provides a reasonable model for the transduction process, we made intracellular cAMP measurements using Fisher rat thyroid cells stably expressing type II vasopressin receptors, FRT-V$_2$R, cultured in F-12 modified Coon's medium (Sigma) supplemented with 10% fetal bovine serum, 100 U/ml penicillin and 100 µg/ml streptomycin at 37°C in a humidified atmosphere of 5% CO$_2$.

FRT-V$_2$R cells were selected every two weeks with medium containing 500 µg/ml Zeocin, 500 µg/ml Geneticin and 350 µg/ml hygromycin. FRT-V$_2$R cells were plated in 24-well plates overnight to obtain 80% confluence. Cells were washed three times with PBS and incubated with 100 nM dDAVP (Sigma-Aldrich), a selective V$_2$R agonist. The incubation time was varied from 5 seconds to 16 minutes and the reaction was terminated by lysis buffer.

Then cell lysate was transferred to 96-well plates for intracellular cAMP measurement using cAMP Biotrak EIA system (Amersham, GE Healthcare). The measurement protocol follows manufacturer's instructions, and samples were determined at optical density 450 nm. The amount of expressed cAMP expressed per unit amount of protein was determined by the Lowry method [18].

Genetic algorithm was then employed to find an optimal set of parametric values for (1)-(3) to yield a solution that best fit our measured time series of expressed cAMP. Using the sum of squares error

$$ss = \sum_{i=1}^{N}\left(C_{t_i}^s - C_{t_i}^d\right)^2$$

for the cost function, where $C_{t_i}^s$ stands for the value of C at time t_i obtained from the model simulation, while $C_{t_i}^d$ is the measured value, N being the number of time points. The genetic algorithm provided us with sets of optimal parametric values corresponding to the least sum of squares. Fig. 2 shows the different simulated time series, corresponding to the four different sets of parametric values for four executions of genetic algorithms.

The simulated curve using the set of parametric values given in (a) in the figure caption appears to provide the best fit to the experimental data ($\lozenge\lozenge\lozenge$). To give some idea of how these predictions could be interpolated, we consider in particular this set of parameters in case (a) in which K_C is found to be $1.7\,\text{fmol}/\,\mu\text{gram}\cdot\text{protein}$, which corresponds to the

y-intercept on the corresponding dose response curve seen in Fig. 2. If we then use the value of value of the cAMP degradation rate k_{-c} quoted in [19] to be $1\;s^{-1}$, then we are led to the apparent zero order synthesis rate

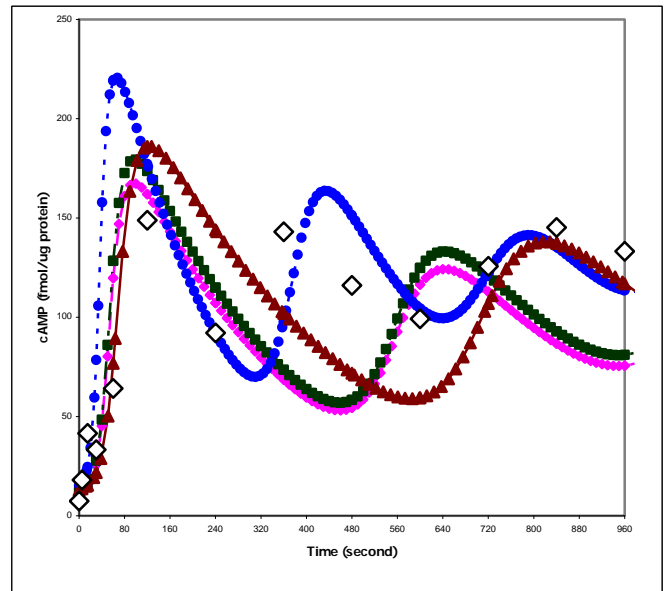$$k_c' = K_C k_{-c} \cong 1.7\;\text{fmol}/\,\mu\text{gram}\cdot\text{protein}.$$

Fig. 2 Plots of the experimental data on expressed cAMP ($\lozenge\lozenge\lozenge$) and simulated time series, with $a_1 = 0.9$, $a_2 = 0.3$, $a_3 = 0.9$, $a_4 = 0.3$, $a_5 = 0.5$, $a_6 = 0.006$, $b_1 = 0.5$, $b_2 = 0.1$,

(a) ● ● ● : $b_3 = 85.001$, $t^* = 67.483$ s , $K_C = 1.70$;

(b) ◆ ◆ ◆ : $b_3 = 64.485$, $t^* = 100.00$ s , $K_C = 1.2897$;

(c) ■ ■ ■ : $b_3 = 69.1277$, $t^* = 100.00$ s , $K_C = 1.3826$;

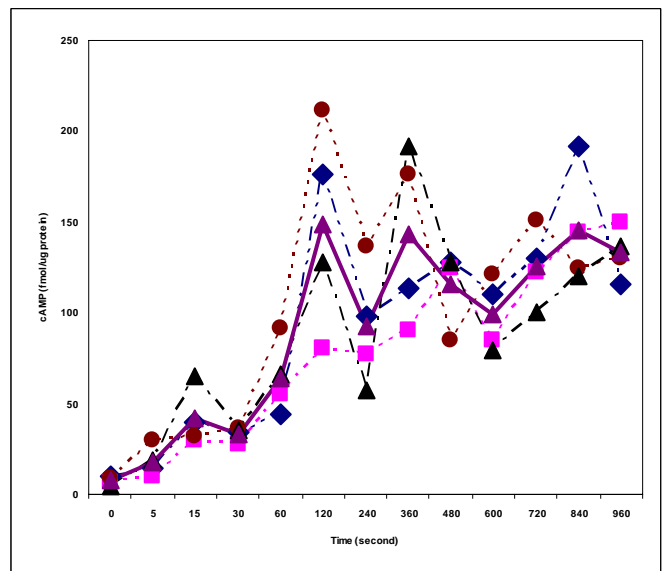(d) ▲ ▲ ▲ : $b_3 = 71.699$, $t^* = 127.457$ s , $K_C = 1.434$.

Fig. 3 Plots of the expressed cAMP measured in 4 experiments under the same controlled conditions. The mean values are plotted as ▲▲ connected by solid lines.

We have in fact carried out several experiments to measure the cAMP levels under the same controlled conditions, as described above. However, we obtained time series which do not follow the same path, or remain reasonably close to each other as time progresses (as seen in Fig. 3). They seem to exhibit different dynamic behavior. Apparently, other factors seem to be operating in the process that potentially leads to different functional responses.

IV. A REACTION DIFFUSION SYSTEM MODEL

Several studies [10-12] have reported that both the inhibiting components and the receptor complexes can diffuse over the cell membrane, and the clustering of these proteins is an essential feature of the transduction process, linked to the various cell functions in response to the signals. Thus, we now allow diffusion at the cellular level in both the inhibitor agents and that of the ligand-receptor complex, and arrive at the following reaction diffusion model equations.

$$\frac{\partial \hat{I}}{\partial \tau} = -a_1 \hat{I} + a_2 \hat{R} + \mu_1 \nabla^2 \hat{I}, \tag{19}$$

$$\frac{\partial \hat{R}}{\partial \tau} = -a_3 \hat{R} - \frac{b_1 \hat{R}}{b_2 + \hat{R}} + \frac{a_4 \hat{R}^2}{\left(a_5 \hat{R} + \hat{I}\right)^2} + a_6 + \mu_2 \nabla^2 \hat{R}, \tag{20}$$

where $\hat{I}$ and $\hat{R}$ now represent the inhibitor and LR complex densities, respectively, at the point (X, Y) on the cell membrane at any time t, while μ_1 and μ_2 are the diffusion coefficients. In (19)-(20), we have introduced a spatial scaling factor d (μm) and let $x = \frac{X}{d}, y = \frac{Y}{d}$ be the dimensionless spatial variables, so that $\nabla = \frac{\partial^2}{\partial x^2} + \frac{\partial^2}{\partial y^2}$.

According to several studies, lateral diffusion coefficient of the inhibiting enzymes in the cytosol has been observed to be significantly higher than that of the membrane receptor complexes. The lateral diffusion coefficients of ligand-receptor complexes have been reported, as early as 1951, by Pastan, and M. Willingham [15] to be in the range of $1.5 \times 10^{-2} - 8 \times 10^{-2}$ $\mu m^2/s$. Later, in 1978, Schlessinger $et\ al.$ [14] reported that the protease inhibitors diffuse within the muscle fibers at the rate of $1\ \mu m^2/s$. This means that the inhibiting units in the transduction process diffuse at a much higher rate than the receptor complex, which allows the application of weakly nonlinear analysis, a technique discussed in detail in [20].

In the next section, we shall carry out a weakly nonlinear stability analysis on (19)-(20) in order to show the existence of hexagonal planform solutions to our model. The readers are referred to the works of Wollkind $et\ al.$ [20] and Stephenson and Wollkind [21] for more discussion of the technique, and to the works of Pansuwan $et\ al.$ [22] for applications of the technique to a different setting.

V. NONLINEAR STABILITY ANALYSES

In order to apply the technique of weakly nonlinear stability theory, we let

$$F\left(\hat{I}, \hat{R}\right) = -a_1 \hat{I} + a_2 \hat{R}, \tag{21}$$

$$G\left(\hat{I}, \hat{R}\right) = -a_3 \hat{R} - \frac{b_1 \hat{R}}{b_2 + \hat{R}} + \frac{a_4 \hat{R}^2}{\left(a_5 \hat{R} + \hat{I}\right)^2} + a_6, \tag{22}$$

which transform (19)-(20) into

$$\hat{I}_\tau = F\left(\hat{I}, \hat{R}\right) + \mu_1 \nabla^2 \hat{I}, \tag{23}$$

$$\hat{R}_\tau = G\left(\hat{I}, \hat{R}\right) + \mu_2 \nabla^2 \hat{R}. \tag{24}$$

Assuming that the system of our referenced model equations (23)-(24) has a unique positive steady state (I_0, R_0), we expand $F\left(\hat{I}, \hat{R}\right)$ and $G\left(\hat{I}, \hat{R}\right)$ into Taylor's series about this steady state. Letting $i \equiv \hat{I} - I_0$, $r \equiv \hat{R} - R_0$, we obtain the following system on i and r:

$$\begin{pmatrix} i \\ r \end{pmatrix}_\tau = \begin{pmatrix} f_1 & f_2 \\ g_1 & g_2 \end{pmatrix} \begin{pmatrix} i \\ r \end{pmatrix} + \begin{pmatrix} 0 & 0 \\ g_3 & g_4 \end{pmatrix} \begin{pmatrix} i^2 \\ r^2 \end{pmatrix} + \begin{pmatrix} 0 \\ g_5 \end{pmatrix} (ir) + \begin{pmatrix} \mu_1 \nabla^2 i \\ \mu_2 \nabla^2 r \end{pmatrix} \tag{25}$$

where,

$f_1 \equiv -a_1$,

$f_2 \equiv a_2$,

$g_1 \equiv -2 a_4 R_0^2 \big/ \left(a_5 R_0 + I_0\right)^3$,

$g_2 \equiv -a_3 - b_3 b_4 \big/ \left(b_4 + R_0\right)^2 + 2 a_4 I_0 R_0 \big/ \left(a_5 R_0 + I_0\right)^3$

$g_3 \equiv 3 a_4 R_0^2 \big/ \left(a_5 R_0 + I_0\right)^4$,

$g_4 \equiv b_3 b_4 \big/ \left(b_4 + R_0\right)^3 + a_4 I_0 \left(-2 a_5 R_0 + I_0\right) \big/ \left(a_5 R_0 + I_0\right)^4$,

$g_5 \equiv -2 a_4 \left(-a_5 R_0^2 + 2 R_0 I_0\right) \big/ \left(a_5 R_0 + I_0\right)^4$.

A. A Hexagonal Planform Analysis

In order to investigate the possibility of occurrence in our model of hexagonal-type patterns, we now consider a hexagonal planform solution of (25) of the form [20,21]

$$\underline{v}(x, y, t) \sim A(t) \cos(q_c x) \underline{v}_{1020}$$

$$+ B(t) \cos\left(\frac{1}{2} q_c x\right) \cos\left(\frac{\sqrt{3}}{2} q_c y\right) \underline{v}_{0111}$$

$$+ A^2(t)[\underline{v}_{2000} + \underline{v}_{2040} \cos(2 q_c x)]$$

$$+ A(t) B(t)[\underline{v}_{1111} \cos\left(\frac{1}{2} q_c x\right) \cos\left(\frac{\sqrt{3}}{2} q_c y\right)$$

$$+ \underline{v}_{1131} \cos\left(\frac{3}{2} q_c x\right) \cos\left(\frac{\sqrt{3}}{2} q_c y\right)]$$

$$+ B^2(t) \begin{bmatrix} \underline{v}_{0200} + \underline{v}_{0220} \cos(q_c x) + \underline{v}_{0202} \cos\left(\sqrt{3} q_c y\right) \\ + \underline{v}_{0222} \cos(q_c x) \cos\left(\sqrt{3} q_c y\right) \end{bmatrix}$$

$$+A^3(t)[\underline{y}_{3020}\cos(q_c x)+\underline{y}_{3060}\cos(3q_c x)]$$

$$+A^2(t)B(t)[\underline{y}_{2111}\cos\left(\frac{1}{2}q_c x\right)\cos\left(\frac{\sqrt{3}}{2}q_c y\right)$$

$$+\underline{y}_{2131}\cos\left(\frac{3}{2}q_c x\right)\cos\left(\frac{\sqrt{3}}{2}q_c y\right)$$

$$+\underline{y}_{2151}\cos\left(\frac{5}{2}q_c x\right)\cos\left(\frac{\sqrt{3}}{2}q_c y\right)]$$

$$+A(t)B^2(t)[\underline{y}_{1200}+\underline{y}_{1220}\cos(q_c x)$$

$$+\underline{y}_{1240}\cos(2q_c x)+\underline{y}_{1202}\cos(\sqrt{3}q_c y)$$

$$+\underline{y}_{1222}\cos(q_c x)\cos(\sqrt{3}q_c y)$$

$$+\underline{y}_{1242}\cos(2q_c x)\cos(\sqrt{3}q_c y)]$$

$$+B^3(t)[\underline{y}_{0311}\cos\left(\frac{1}{2}q_c x\right)\cos\left(\frac{\sqrt{3}}{2}q_c y\right)$$

$$+\underline{y}_{0331}\cos\left(\frac{3}{2}q_c x\right)\cos\left(\frac{\sqrt{3}}{2}q_c y\right)$$

$$+\underline{y}_{0313}\cos\left(\frac{1}{2}q_c x\right)\cos\left(\frac{3\sqrt{3}}{2}q_c y\right)$$

$$+\underline{y}_{0333}\cos\left(\frac{3}{2}q_c x\right)\cos\left(\frac{3\sqrt{3}}{2}q_c y\right)], \tag{26}$$

where

$$\underline{y}(x,y,t)\equiv\begin{pmatrix}i(x,y,t)\\r(x,y,t)\end{pmatrix},\ \underline{y}_{j\ell mn}\equiv\begin{pmatrix}i_{j\ell mn}\\r_{j\ell mn}\end{pmatrix}$$

with the amplitude equations:

$$\frac{dA(t)}{dt}\simeq\sigma A(t)-\alpha_0 B^2(t)-A(t)[\alpha_1 A^2(t)+\alpha_2 B^2(t)], \tag{27}$$

$$\frac{dB(t)}{dt}\simeq\sigma B(t)-4\alpha_0 A(t)B(t)-B(t)[2\alpha_2 A^2(t)$$
$$+\frac{1}{4}(\alpha_1+2\alpha_2)B^2(t)]. \tag{28}$$

Here, we are employing the notation $\underline{y}_{j\ell mn}$ for the coefficient of each term in (26) of the form

$$A^j(t)B^\ell(t)\cos\left(\frac{mq_c x}{2}\right)\cos\left(\frac{n\sqrt{3}q_c y}{2}\right). .$$

Substituting this solution in (26) into (25) and equating coefficients of like-terms, we obtain a sequence of vector systems, each of which corresponds to one of these terms. In particular, the first order system which corresponds to $j=m=1$, $l=n=0$ is

$$\sigma\underline{y}_{1020}=\begin{pmatrix}f_1-q_c^2\mu_1 & f_2\\g_1 & g_2-q_c^2\mu_2\end{pmatrix}\underline{y}_{1020},$$

so that

$$\sigma^2-\left(f_1-q_c^2\mu_1+g_2-q_c^2\mu_2\right)\sigma$$
$$+\left[\left(f_1-q_c^2\mu_1\right)\left(g_2-q_c^2\mu_2\right)-f_2 g_1\right]=0,$$

and thus,

$$\sigma=\frac{\left(f_1-q_c^2\mu_1+g_2-q_c^2\mu_2\right)\pm\sqrt{\begin{array}{c}\left(f_1-q_c^2\mu_1+g_2-q_c^2\mu_2\right)^2\\-4\left[\left(f_1-q_c^2\mu_1\right)\left(g_2-q_c^2\mu_2\right)-f_2 g_1\right]\end{array}}}{2}.$$

Letting $\sigma=\sigma_0$ be the growth rate of the most dangerous mode,

$$\sigma_0=\frac{\left(f_1-q_c^2\mu_1+g_2-q_c^2\mu_2\right)+\sqrt{\begin{array}{c}\left(f_1-q_c^2\mu_1+g_2-q_c^2\mu_2\right)^2\\-4\left[\left(f_1-q_c^2\mu_1\right)\left(g_2-q_c^2\mu_2\right)-f_2 g_1\right]\end{array}}}{2},$$

and then

$$\underline{y}_{1020}=\begin{pmatrix}i_{1020}\\r_{1020}\end{pmatrix}$$

is an eigenvector corresponding to the eigenvalue $\sigma=\sigma_0$, where

$$i_{1020}=f_2,$$

and

$$r_{1020}=\sigma-f_1+q_c^2\mu_1.$$

Similarly, the first order system which corresponds to $j=m=0$, $\ell=n=1$ is

$$\sigma\underline{y}_{0111}=M\underline{y}_{0111}.$$

Therefore, without loss of generality, we take

$$\underline{y}_{0111}=\underline{y}_{1020}.$$

There are eight second-order systems, two of which contain the Landau constant α_0. We can express one of them as

$$2\sigma\underline{y}_{0220}=\alpha_0\underline{y}_{1020}+M\underline{y}_{0220}+\begin{pmatrix}0\\\frac{1}{4}\left(g_3 i_{0111}^2+g_4 r_{0111}^2+g_5 i_{0111}r_{0111}\right)\end{pmatrix}. \tag{29}$$

Considering the adjoint linear eigenvalue problem of (29):

$$M^T\underline{y}^*=\sigma^*\underline{y}^*,$$

where $\sigma^*=\sigma$ is an eigenvalue of M and M^T, we obtain

$$\underline{y}^*=\begin{pmatrix}g_1\\\sigma-f_1+\mu_1 q_c^2\end{pmatrix}.$$

By taking an inner product of (29) with $\underline{y}^*$, we find, upon making use of the adjoint property

$$M\underline{y}\cdot\underline{y}^*=\underline{y}\cdot M^T\underline{y}^*=\sigma\underline{y}\cdot\underline{y}^*$$

that

$$2\sigma\underline{y}_{0220}\cdot\underline{y}^*=\alpha_0\underline{y}_{1020}\cdot\underline{y}^*+\sigma\underline{y}_{0220}\cdot\underline{y}^*$$
$$+\begin{pmatrix}0\\\frac{1}{4}\left(g_3 i_{0111}^2+g_4 s_{0111}^2+g_5 i_{0111}r_{0111}\right)\end{pmatrix}\cdot\underline{y}^*$$

Then, taking the limit as $\sigma\to 0$, we obtain

$$\alpha_0=-\frac{1}{4}\left[\frac{\left(g_3 i_{0111}^2+g_4 s_{0111}^2+g_5 i_{0111}s_{0111}\right)\left(-f_1+\mu_1 q_c^2\right)}{g_1 i_{1020}+\left(-f_1+\mu_1 q_c^2\right)s_{1020}}\right]\Bigg|_{\sigma\to 0}.$$

The other six second-order systems can be solved in a straight forward manner, the solutions being

$$i_{2000} = \frac{f_2}{2}\left[\frac{g_3 i_{1020} + g_4 r_{1020} + g_5 i_{1020} r_{1020}}{(2\sigma - f_1)(2\sigma - g_2) - f_2 g_1}\right],$$

$$r_{2000} = \frac{1}{f_2}(2\sigma - f_1)i_{2000},$$

$$i_{2040} = \frac{f_2}{2}\left[\frac{g_3 i_{1020} + g_4 r_{1020} + g_5 i_{1020} r_{1020}}{(2\sigma - f_1 + 4\mu_1 q_c^2)(2\sigma - g_2 + 4\mu_2 q_c^2) - f_2 g_1}\right],$$

$$r_{2040} = \frac{1}{f_2}(2\sigma - f_1 + 4\mu_1 q_c^2)i_{2040},$$

$$i_{0200} = \frac{f_2}{4}\left[\frac{g_3 i_{0111}^2 + g_4 r_{0111}^2 + g_5 i_{0111} r_{0111}}{(2\sigma - f_1)(2\sigma - g_2) - f_2 g_1}\right],$$

$$r_{0200} = \frac{1}{f_2}(2\sigma - f_1)i_{0200},$$

$$i_{0220} = \left[\frac{\alpha_0\left[(2\sigma - g_2 + \mu_2 q_c^2)i_{1020} + f_2 r_{1020}\right] + \frac{f_2}{4}(g_3 i_{0111}^2 + g_4 r_{0111}^2 + g_5 i_{0111} r_{0111})}{(2\sigma - f_1 + 4\mu_1 q_c^2)(2\sigma - g_2 + 4\mu_2 q_c^2) - f_2 g_1}\right],$$

$$r_{0220} = \frac{1}{f_2}\left[(2\sigma - f_1 + \mu_1 q_c^2)i_{0220} - \alpha_0 i_{1020}\right],$$

$$i_{1111} = \left[\frac{2\alpha_0\left[\left(\sigma - g_2 + \frac{1}{2}\mu_2 q_c^2\right)i_{0111} + f_2 r_{0111}\right] + \frac{f_2}{2}(g_3 i_{0111}^2 + g_4 r_{0111}^2 + g_5 i_{0111} r_{0111})}{\left(\sigma - f_1 + \frac{1}{2}\mu_1 q_c^2\right)\left(\sigma - g_2 + \frac{1}{2}\mu_2 q_c^2\right) - f_2 g_1}\right],$$

$$r_{1111} = \frac{1}{f_2}\left[\left(\sigma - f_1 + \frac{1}{2}\mu_1 q_c^2\right)i_{1111} - 2\alpha_0 i_{0111}\right],$$

$$i_{1131} = \frac{f_2}{2}\left[\frac{g_3 i_{0111}^2 + g_4 r_{0111}^2 + g_5 i_{0111} r_{0111}}{\left(\sigma - f_1 + \frac{3}{2}\mu_1 q_c^2\right)\left(\sigma - g_2 + \frac{3}{2}\mu_2 q_c^2\right) - f_2 g_1}\right],$$

$$r_{1131} = \frac{1}{f_2}\left(\sigma - f_1 + \frac{3}{2}\mu_1 q_c^2\right)i_{1131}.$$

Although there are 15 third-order systems, it is necessary for us to consider explicitly only the following two specific ones, which contain the other two Landau constants α_1, α_2 as:

$$3\sigma \underline{v}_{3020} = \alpha_1 \underline{v}_{1020} + M\underline{v}_{3020}$$
$$+ \begin{pmatrix} 0 \\ \left(2g_3 i_{2000} + g_3 i_{2040} + g_5 r_{2000} + \frac{1}{2}g_5 r_{2040}\right)i_{1020} \end{pmatrix}$$
$$+ \begin{pmatrix} 0 \\ \left(2g_4 r_{2000} + g_4 r_{2040} + g_5 i_{2000} + \frac{1}{2}g_5 i_{2040}\right)r_{1020} \end{pmatrix}. \tag{30}$$

and

$$3\sigma \underline{v}_{1220} = \alpha_2 \underline{v}_{1020} + 8\alpha_0 \underline{v}_{0220} + M\underline{v}_{1220}$$
$$+ \begin{pmatrix} 0 \\ \left(2g_3 i_{0200} + g_5 r_{0200}\right)i_{1020} + \left(2g_4 r_{0200} + g_5 i_{0200}\right)r_{1020} \end{pmatrix}$$
$$+ \begin{pmatrix} 0 \\ \left(\frac{1}{2}g_3 i_{1111} + \frac{1}{4}g_3 i_{1131} + \frac{1}{4}g_5 r_{1111} + \frac{1}{4}g_5 r_{1131}\right)i_{0111} \end{pmatrix}$$
$$+ \begin{pmatrix} 0 \\ \left(\frac{1}{2}g_4 r_{1111} + \frac{1}{4}g_4 r_{1131} + \frac{1}{4}g_5 i_{1111} + \frac{1}{4}g_5 i_{1131}\right)r_{0111} \end{pmatrix}. \tag{31}$$

Considering the adjoint linear eigenvalue problem of (30)-(31):

$$M^T \underline{v}^* = \sigma^* \underline{v}^*,$$

where $\sigma^* = \sigma$ is an eigenvalue of M and M^T, then

$$\underline{v}^* = \begin{pmatrix} g_1 \\ \sigma - f_1 + \mu_1 q_c^2 \end{pmatrix}.$$

By taking inner products of (30) and (31) with $\underline{v}^*$, we find, upon making use of the adjoint property

$$M\underline{v} \cdot \underline{v}^* = \underline{v} \cdot M^T \underline{v}^* = \sigma \underline{v} \cdot \underline{v}^*$$

that

$$3\sigma \underline{v}_{3020} \cdot \underline{v}^* = \alpha_1 \underline{v}_{1020} \cdot \underline{v}^* + \sigma \underline{v}_{3020} \cdot \underline{v}^*$$
$$+ \begin{pmatrix} 0 \\ \left(2g_3 i_{2000} + g_3 i_{2040} + g_5 r_{2000} + \frac{1}{2}g_5 r_{2040}\right)i_{1020} \end{pmatrix} \cdot \underline{v}^*$$
$$+ \begin{pmatrix} 0 \\ \left(2g_4 r_{2000} + g_4 r_{2040} + g_5 i_{2000} + \frac{1}{2}g_5 i_{2040}\right)r_{1020} \end{pmatrix} \cdot \underline{v}^*,$$

and

$$3\sigma \underline{v}_{1220} \cdot \underline{v}^* = \alpha_2 \underline{v}_{1020} \cdot \underline{v}^* + 8\alpha_0 \underline{v}_{0220} \cdot \underline{v}^* + \sigma \underline{v}_{1220} \cdot \underline{v}^*$$
$$+ \begin{pmatrix} 0 \\ \left(2g_3 i_{0200} + g_5 r_{0200}\right)i_{1020} + \left(2g_4 r_{0200} + g_5 i_{0200}\right)r_{1020} \end{pmatrix} \cdot \underline{v}^*$$
$$+ \begin{pmatrix} 0 \\ \left(\frac{1}{2}g_3 i_{1111} + \frac{1}{4}g_3 i_{1131} + \frac{1}{4}g_5 r_{1111} + \frac{1}{4}g_5 r_{1131}\right)i_{0111} \end{pmatrix} \cdot \underline{v}^*$$
$$+ \begin{pmatrix} 0 \\ \left(\frac{1}{2}g_4 r_{1111} + \frac{1}{4}g_4 r_{1131} + \frac{1}{4}g_5 i_{1111} + \frac{1}{4}g_5 i_{1131}\right)r_{0111} \end{pmatrix} \cdot \underline{v}^*. \tag{30}$$

Then, taking the limit as $\sigma \to 0$, we obtain

$$\alpha_1 = -\frac{\left[\left(2g_3i_{2000}+g_3i_{2040}+g_5r_{2000}+\frac{1}{2}g_5r_{2040}\right)i_{1020}\right]\left[-f_1+\mu_1q_c^2\right]}{g_1i_{1020}+\left(-f_1+\mu_1q_c^2\right)r_{1020}}\Bigg|_{\sigma\to 0}$$

$$-\frac{\left[\left(2g_4r_{2000}+g_4r_{2040}+g_5i_{2000}+\frac{1}{2}g_5i_{2040}\right)r_{1020}\right]\left[-f_1+\mu_1q_c^2\right]}{g_1i_{1010}+\left(-f_1+\mu_1q_c^2\right)r_{1010}}\Bigg|_{\sigma\to 0}$$

and

$$\alpha_2 = -\frac{8\alpha_0\left[g_1i_{0220}+\left(-f_1+\mu_1q_c^2\right)r_{0220}\right]}{g_1i_{1020}+\left(-f_1+\mu_1q_c^2\right)r_{1020}}\Bigg|_{\sigma\to 0}$$

$$-\frac{\left[\begin{array}{c}\left(2g_3i_{0200}+g_5r_{0200}\right)i_{1020}\\+\left(2g_4r_{0200}+g_5i_{0200}\right)r_{1020}\end{array}\right]\left[-f_1+\mu_1q_c^2\right]}{g_1i_{1020}+\left(-f_1+\mu_1q_c^2\right)r_{1020}}\Bigg|_{\sigma\to 0}$$

$$-\frac{\left[\left(\frac{1}{2}g_3i_{1111}+\frac{1}{4}g_3i_{1131}+\frac{1}{4}g_5r_{1111}+\frac{1}{4}g_5r_{1131}\right)i_{0111}\right]\left[-f_1+\mu_1q_c^2\right]}{g_1i_{1020}+\left(-f_1+\mu_1q_c^2\right)r_{1020}}\Bigg|_{\sigma\to 0}$$

$$-\frac{\left[\left(\frac{1}{2}g_4r_{1111}+\frac{1}{4}g_4r_{1131}+\frac{1}{4}g_5i_{1111}+\frac{1}{4}g_5i_{1131}\right)r_{0111}\right]\left[-f_1+\mu_1q_c^2\right]}{g_1i_{1020}+\left(-f_1+\mu_1q_c^2\right)r_{1020}}\Bigg|_{\sigma\to 0}.$$

Having developed these formulae for the Landau constants, we now turn our attention to the hexagonal planform amplitude equations (17)-(18) which possess the following equivalence classes of critical points (A_0, B_0) when $q_c^2 = 1$:

$$\text{I}: A_0 = B_0 = 0; \tag{32}$$

$$\text{II}: A_0^2 = \sigma/\alpha_1, \ B_0 = 0; \tag{33}$$

$\text{III}^{\pm}$:

$$A_0 = B_0 = A_0^{\pm}$$
$$= \left\{-2\alpha_0 \pm \left[4\alpha_0^2 + (\alpha_1+4\alpha_2)\sigma\right]^{\frac{1}{2}}\right\}\Big/(\alpha_1+4\alpha_2); \tag{34}$$

$$\text{IV}: A_0 = -4\alpha_0/(2\alpha_2-\alpha_1), \ B_0 = (\sigma-\sigma_1)/(\alpha_1+2\alpha_2), \tag{35}$$

where we are assuming that $\alpha_1 > 0$, and

$$\alpha_1 + 4\alpha_2 > 0$$

with

$$\sigma_{-1} \equiv -4\alpha_0^2/(\alpha_1+4\alpha_2),$$
$$\sigma_1 \equiv 16\alpha_1\alpha_0^2/(2\alpha_2-\alpha_1)^2,$$

and

$$\sigma_2 \equiv 32(\alpha_1+\alpha_2)\alpha_0^2/(2\alpha_2-\alpha_1)^2.$$

The orbital stability conditions for these critical points can be posed in terms of σ. This sort of stability of pattern formation is meant in the sense of a family of solution in the plane which may interchange with each other but do not grow or decay to a solution type from a different family. Such an interpretation depends upon the translational and rotational symmetries inherent to the amplitude-phase equations. This invariance also limits each equivalence class of critical points to a single member that must be explicitly considered.

Table 1: Orbital stability behavior of critical points II and III$^{\pm}$

α_0	$2\alpha_2-\alpha_1$	Stable Structures
$+$	$-, 0$	III$^-$ for $\sigma > \sigma_{-1}$
$+$	$+$	III$^-$ for $\sigma_{-1} < \sigma < \sigma_2$, II for $\sigma > \sigma_1$
0	$-$	III$^{\pm}$ for $\sigma > 0$
0	$+$	II for $\sigma > 0$
$-$	$+$	III$^+$ for $\sigma_{-1} < \sigma < \sigma_2$, II for $\sigma > \sigma_1$
$-$	$-, 0$	III$^+$ for $\sigma > \sigma_{-1}$

Thus, critical point I is stable in this sense that $\sigma < 0$ while the stability behavior II and III$^{\pm}$, which depends upon the signs of α_0 and $2\alpha_2-\alpha_1$ as well, has been summarized in Table 1 under the further assumption that $\alpha_1 + \alpha_2 > 0$.

The critical point VI is always unstable, as may be seen from considering (35).

B. Morphological Interpretation

We next offer a morphological interpretation of the potentially stable critical points described above relative to the Turing patterns under investigation. To the lowest order, the solution of the model associated with these critical points is given by

$$r \sim A_0\cos(x)r_{1020} + 2B_0\cos\left(\frac{1}{2}x\right)\cos\left(\frac{\sqrt{3}}{2}y\right)r_{0111}. \tag{36}$$

Then, the critical point I represents the uniform or homogeneous state, while the stripes or bands corresponds to critical point II.

These contour plots of (36) are presented in figures 4, 5, and 6 for critical points II, III$^+$ and III$^-$, respectively, in which elevations appear dark and depressions light. Clearly, such

alternating light and dark parallel bands produced by the critical point II should be identified with a striped Turing pattern as seen in Fig. 4.
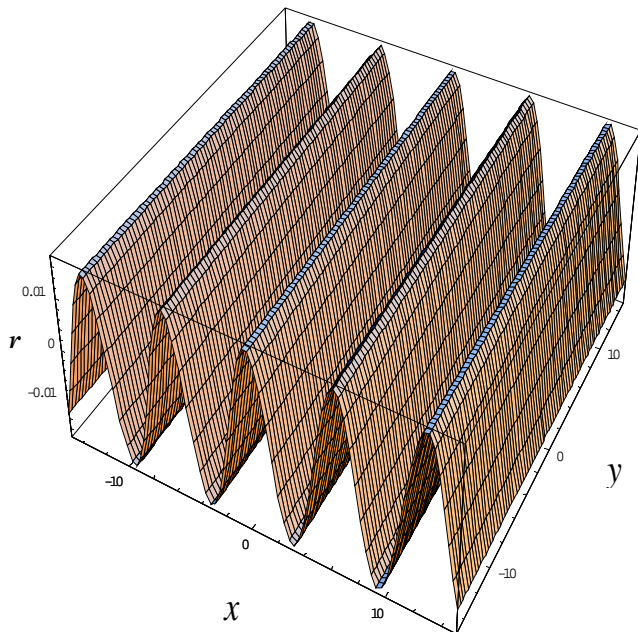

Fig. 4 Contour plot of (36) for the critical point II with $a_1 = a_2 = a_4 = a_5 = a_6 = 0.1, a_3 = 0.5, b_1 = 0.1, b_2 = 0.1, \mu_1 = 0.9, \mu_2 = 0.0001,$ $q_c^2 = 1$. The stable morphology in this case is the striped pattern.
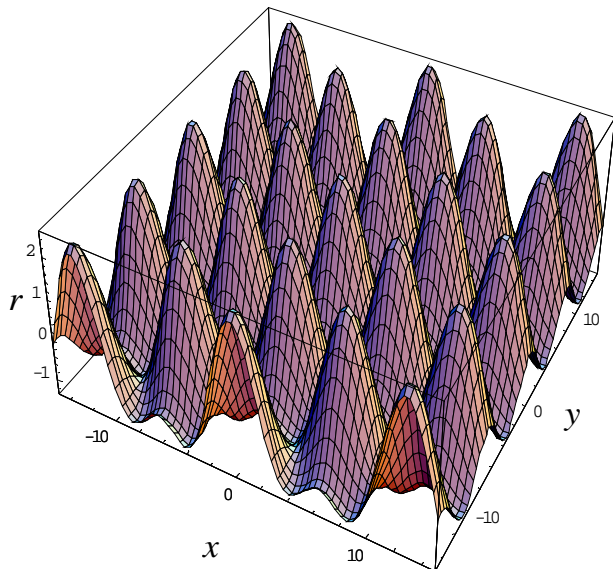

Fig. 5 Contour plot of (36) for the critical point III^+ with $a_1 = 0.1, a_2 = 0.1, a_3 = 0.5, a_4 = 0.1, a_5 = 0.1, \ a_6 = 0.1, b_1 = 0.1, b_2 = 0.1,$ $\mu_1 = 0.9, \mu_2 = 0.1, \ q_c^2 = 1$. The stable morphology in this case is the hexagonal arrays of dots (quantum dots).

Focusing our attention on the contour plot in Fig. 5, we observe that each individual r cell has an elevated nearly circular central region whose height is maximum at its centre.

It is surrounded by a level curve of zero height. The region surrounding each cell exterior to the central portion is depressed with the hexagonal cellular boundary. The depth of this boundary is seen to vary from being the greatest at its vertices to being the least at its edges. Since $A_0^+ > 0$ for $\alpha_0 \leq 0$ and $A_0^- < 0$ for $\alpha_0 \geq 0$, we can conclude that the contour plots of (36) would have circular elevations at the centers of the hexagonals for critical point III^+ when stable, and circular depression for III^-.
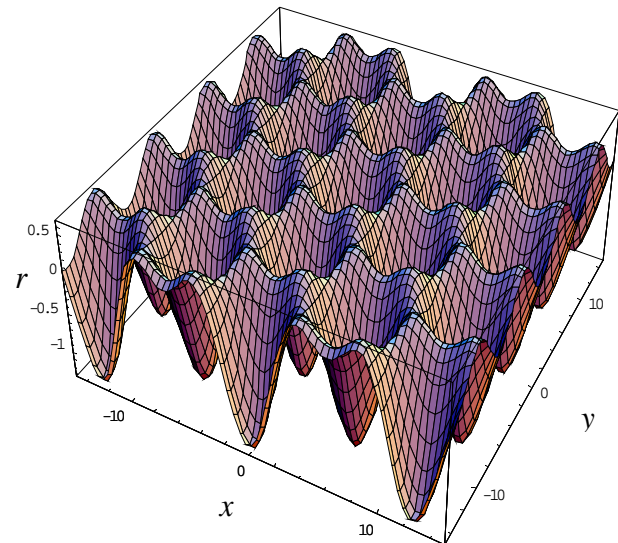

Fig. 6 Contour plot of (36) for the critical point III^- with $a_1 = 0.5, a_2 = 0.5, a_3 = 0.5, a_4 = 0.3, a_5 = 0.1, a_6 = 0.1, b_1 = 0.1,$ $b_2 = 0.1, \mu_1 = 0.9, \mu_2 = 0.005, \ q_c^2 = 1$. The stable morphology in this case is the hexagonal arrays of holes (or honey combs).

Recalling that the Turing patterns under consideration are classified by their elevations, we identify hexagonal arrays of nets or honeycombs with critical point III^+ and of spots or dots with critical point III^- shown in Fig. 6.

VI. DISCUSSION AND CONCLUSION

We have utilized a weakly nonlinear stability analysis in order to predict pattern selection of membrane receptors. The procedure basically pivots a perturbation about the critical point of linear stability theory. The nonlinear terms are responsible for selecting which of the possible spatial patterns are actually observed. As commented by Wollkind *et al.* in their review of this method [20], this approach has an advantage over strictly numerical procedures since it allows us to derive quantitative relationships between the system parameters and the stable patterns so that insightful deductions can more readily be made concerning the connections between different types of spatial selections and the cellular functional

response, especially when experiments need to be designed to validate theoretical predictions, a task difficult to accomplish using numerical simulation alone.

To make a connection between reported experimental measurements and our predictions of different LR complex distribution patterns on the cell membrane, we refer to the work of Schlessinger *et al.* [14] which stated that the protease inhibitors diffuse within the muscle fibers at the rate

$$\mu_1 = 10^{-8} \, \text{cm}^2 / \text{s},$$

while Patricio Catricio Carvajal-Rondanelli [23] reported that insulin diffuses at

$$\mu_2 = 10^{-10} \, \text{cm}^2 / \text{s}.$$

This means that

$$\mu_1 / \mu_2 = 10^2.$$

Considering this ratio from our predictions, it is

$$\mu_1 / \mu_2 \cong 0.9 / 0.1 \cong 10$$

for quantum dots to occur, while we require

$$\mu_1 / \mu_2 \cong 0.9 / 0.005 \cong 1.8 \times 10^2$$

for honeycombs. Thus, our model predicts a formation of hexagonal arrays of holes or honeycombs in such a case, provided that other physical parameters could be controlled to be in the respective ranges that allow the formation of this Turing pattern.

On the other hand, Schlessinger *et al.* [14] reported that the protease inhibitors diffuse in cells in aqueous solution at the rate

$$\mu_1 = 10^{-6} \, \text{cm}^2 / \text{s}.$$

Thus, in this case we have

$$\mu_1 / \mu_2 = 10^4.$$

For a formation of stripes as seen in Fig. 2, $\mu_1 = 0.9$ and $\mu_1 = 0.0001$, so that stripes formation corresponds to a ratio

$$\mu_1 / \mu_2 \cong 0.9 / 0.0001 \cong 9 \times 10^3 \cong 10^4.$$

Hence, stripes are the predicted morphology on such cell surface in aqueous solutions, provided that other physical parameters could be controlled to be in the respective ranges that allow the formation of this Turing pattern.

To date, only limited numbers of studies have been published in terms of pictured spatial distribution of membrane receptor complexes. However, with recent advances in imaging techniques and computer technology, many investigators have reported their findings concerning immobilization or membrane distribution of receptors of crucial importance.

Rhodopsin was the first member of the family of 7-helix receptors to have its structure determined by X-ray crystallography. Perhaps for this reason, more images may be found in the literature of rhodopsin distribution and alignment on the plasma membrane, although no attempt has yet been made, to our knowledge, to relate different spatiotemporal patterns of these receptors to the various functional cellular responses.

For example, in 2002 Orem and Dolph [24] reported on their investigation of the localization of photoreceptor cell-specific proteins during endocytosis-mediated retinal degeneration. In their study, flies were treated with 24 h of room light and retinas were dissected. The retinas were then heated with 15

min of either blue light to convert rhodopsin to the M form, or orange light to convert the rhodopsin to the inactive form. After the light treatment of 24 h, the rhodopsin monoclonal antibody only recognizes the rhodopsin that has been inactivated by orange light [24]. Their paper presented images of rhodopsin distribution which resembles striped as well as hexagonal patterns of clustering.

It has been often documented that altered receptor localization or ligand-induced receptor clustering may regulate receptor functions and signal responses [13, 25-29]. Specifically, Yang *et al.* [29] used a combination of microscopy approaches and mathematical modeling to explore the early steps in receptor signaling. They mapped distributions of a family of growth factor receptors on membranes of breast cancer cells by immuno-electron microscopy. Their results indicate that membrane spatial organization is a contributor to the carcinogenesis process, particularly at moderate expression levels.

In 2003, H. Pick *et al.* [30] reported on their study in which the ionotropic $5HT_3$ receptor was expressed in transiently transfected mammalian cells. They continuously observed receptor traffic in the plasma membrane of live cells over 24 h by fluorescence scanning confocal microscopy. According to this investigation, the receptors started to aggregate in patches with a 4-fold increased surface concentration. An image, by fluorescence scanning confocal microscopy, of such cell surface expression and clustering of $5HT_3$ receptors was clearly observed in the images presented in their report [30]. Their work provides an important evidence of receptors trafficking and clustering in response to ligand binding, although higher resolution is needed to clearly differentiate between various distribution patterns on the cell surface and possibly identify the different types of Turing patterns predicted in this work. Later, in their attempt to link receptor complexes interactions with functional response, Jankevics *et al.* [31] obtained dose-response curves of different ligands for each receptor interaction, using the novel method based on fluorescence correlation spectroscopy which was demonstrated to be suitable for the investigation of multiple protein interactions in vivo at native expression levels in relation to cell response and functions. Such experiments are hoped to open new routes to elucidate transcription regulation and detecting or distinguishing different compounds in terms of their pharmacological or toxicological activities.

A challenge of current biology is to understand how intracellular and intercellular regulatory networks are governed. Activation of signal transduction networks by extracellular stimuli is connected to complex temporal and spatial patterns of activation and localization of numerous proteins that characterize crucial cellular discussion ranging from cell growth and proliferation, growth arrest, differentiation, apoptosis, or cell survival. Our current understanding of spatio-temporal organization in signaling pathways and the control of cellular topology, diffusion and intracellular responses, however, is far from complete [13].

Our model analysis is meant to provide a valuable theoretical ground work on which the relevance of Turing-type pattern formation to signaling processes may be further explored in the hope of shedding more light on the precise

manner in which spatio-temporal organization of multiple component signal transduction cascades may contribute to signals generation with high fidelity and efficiency.

REFERENCES

[1] P.A. Iglesias, "Feedback control in intracellular signaling pathways: regulating chemotaxis in Dictyostelium Discoideum," *Europ. J. Contr.*, vol. 9, pp. 216-225, 2003.

[2] J. Krishnan and P.A. Iglesias, "Analysis of the signal transduction properties of a module of spatial sensing in eukaryotic chemotaxis," *Bull. Math. Biol.*, vol. 65, pp.95-128, 2003.

[3] R.R. Neubig and D.P. Siderovski, "Regulators of G-protein signaling as new central nervous system drug targets," *Nature Rev.*, vol. 1, pp.187-197, 2002.

[4] R.S. Ostrom, X. Liu, B.P. Head, C. Gregorian, T.M. Seasholtz and P.A. Insel, "Localization of adenylyl cyclase isoforms and G protein-coupled receptors in vascular smooth muscle cells: expression in caveolin-rich and noncaveolin domain," *Mol. Pharmacol.*, vol. 62, pp.983-992, 2002.

[5] C. Rattanakul, J. Bell, V. Chatsudthipong, P.S. Crooke and Y. Lenbury, "Spatial Turing-type pattern formation in a model of signal transduction involving membrane-based receptors coupled by G Proteins," *Cancer Informatics*, vol. 2, pp.1-15, 2006.

[6] E.M. Rauch and M.M. Millonas, "The role of trans-membrane signal transduction in turing-type cellular pattern formation," *J. Theor. Biol.*, vol. 226, pp.01-407, 2004.

[7] A.M. Spiegel, "G protein defects in signal transduction," *Horm. Res.*, vol. 53(3), pp.17-22, 2000.

[8] A. Levchenko and P. Iglesias, "Models of eukaryotic gradient sensing: application to chemotaxis of amoebae and neutrophils," *Biophys J.*, vol. 82, pp.50-63, 2002.

[9] W.J. Rappel, P.J. Thomas, H. Levine and W.F. Loomis, "Establishing direction during chemotaxis in eukaryotic cells," *Biophys. J.*, vol. 83, pp.361-1367, 2002.

[10] E.N. Pugh, Jr. and T.D. Lamb, "Amplification and kinetics of the activation steps in phototransduction," *Biochim. Biophys. Acta*, vol. 1141, pp.111-149, 1993.

[11] T.D. Lamb, "Stochastic simulation of activation in the G-protein cascade of vision," *Biophys. J.*, vol. 67, pp.1439-1454, 1994.

[12] S. Ramanathan, P.B. Detwiler, A.M. Sengupta and B.I. Shraiman, "G-protein-coupled enzyme cascades have intrinsic properties that improve signal localization and fidelity," *Biophys. J.*, vol. 88, pp.3063-3071, 2005.

[13] B.N. Kholodenko, "Four-dimensional organization of protein kinase signaling cascades: the roles of diffusion, endocytosis and molecular motors," *J. Exp. Bio.*, vol. 206, pp. 2073-2082, 2003.

[14] J. Schlessinger, Y. Shechter, P. Cuatrecesas, M.C. Willingham and I. Pastan, "Quantitative determinanation of the lateral diffusion coefficients of the hormone-receptor complexes of insulin and epidermal growth factor on the plasma membrane of cultured fibroblasts," *Proc. Natl. Acad. Sci. USA.*, vol. 75(11), pp.5353-5357, 1978.

[15] I. Pastan and M. C. Willingham, *Endocytosis*, Plenum Press, New York, 1985.

[16] H. Lodish, A. Berk, S.L. Zipursky, P. Maatsudaira, D. Baltimore and J. Darnell, *Molecular cell biology*, 4th Ed. W.H. Freeman, New York, pp.849-877, 2000.

[17] A.W. Norman and G. Litwack, *Hormones*. Academic Press, California, USA, 1997.

[18] O.H. Lowry, N.J. Rosebrough, A.L. Farr and R.J. Randall, "Protein measurement with the Folin phenol reagent," *J. Biol. Chem.*, vol. 193, pp.265-75, 1951.

[19] M. Postma and P. J. Van Haastert, "A diffusion-translocation model for gradient sensing by chemotactic cells," *Biophys J.*, vol. 81(3), pp.1314-1323, 2001.

[20] D.J. Wollkind, V.S. Manoranjan and L. Zhang, "Weakly Nonlinear Stability Analyses of Prototype Reaction-Diffusion Model Equations," *Siam Review.*, vol. 36(2), pp.176-214, 1994.

[21] L.E. Stephenson and D.J. Wollkind, "Weakly nonlinear stability analyses of one-dimensional Turing pattern formation in activator-inhibitor/immobilizer model systems," *J. Math. Biol.*, vol. 33, pp.771-815, 1995.

[22] A. Pansuwan, C. Rattanakul, Y. Lenbury, D.J. Wollkind, L. Harrison and I. Rajapakse, "Nonlinear Stability Analyses of Pattern Formation on Solid Surfaces During Ion-Sputtered Erosion," *Mathematical and Computer Modelling*, vol. 41, pp.939-964, 2005.

[23] P.A.Carvajal-Rondanelli, http://en.scientificcommons.org/7723638, 2002.

[24] N.R. Orem and P.J. Dolph, "Epitope masking of rhabdomeric rhodopsin during endocytosis-induced retinal degeneration," *Mol. Vis.*, vol. 8, pp.455-461, 2002.

[25] T. Uyemura, H. Takagi, T. Yanagida and Y. Sako, "Single-molecule analysis of epidermal growth factor signaling that leads to ultrasensitive calcium response," *Biophys. J.*, vol.88, pp.3720-3730, 2005.

[26] J. Zhang, K. Leiderman, J.R. Pfeiffer, B.S. Wilson, J.M. Oliver and S.L. Steinberg, "Charaterizing the topography of membrane receptors and signaling molecules from spatial patterns obtained using nanometer-scale electron-dense probes and electron microscopy," *Micron.*, vol. 37(1), pp.14-34, 2006.

[27] I. Tamir, R.S. Stenner and I. Pecht, "Immobilization of the type I receptor for IgE initiates signal transduction in mast cells," *Biochem.*, vol. 35(21), pp.6872-6883, 1996.

[28] C. Guo and H. Levine, "A thermodynamic model for receptor clustering," *Biophys. J.*, vol. 77(5), pp. 2358-2365, 1999.

[29] S. Yang, M.A. Raymond-Stintz, W. Ying, J. Zhang, D. S. Lidke, S. L. Steinberg, L. Williams, J. M. Oliver and B. S. Wilson, *Journal of Cell Science*, vol. 120, pp. 2763-73, 2007.

[30] H. Pick, A. K. Preuss, M. Mayer, T. Wohland, R. Hovius and H. Vogel, "Monitoring Expression and Clustering of the Ionotropic 5HT3 Receptor in Plasma Membranes of Live Biological Cells," *Biochemistry*, vol. 42 (4), pp.877–884, 2003.

[31] H. Jankevics, M. Prummer, P. Izewska, H. Pick, K. Leufgen and H. Vogel, "Diffusion-time distribution analysis reveals characteristic ligand-dependent interaction patterns of nuclear receptors in living cells," *Biochemistry*, vol. 44(35), pp.11676-83, 2005.